J Mater Sci (2007) 42:5641–5646
DOI 10.1007/s10853-006-0629-z

Studies on the preparation and structure of polyacrylamide/α-zirconium phosphate nanocomposites

Rui Zhang · Yuan Hu · Baoguang Li · Zuyao Chen · Weicheng Fan

Received: 16 November 2005 / Accepted: 27 June 2006 / Published online: 29 March 2007

Abstract In this paper, a novel polyacrylamide(PAM)/α-zirconium phosphate(α-ZrP) nanocomposite was successfully synthesized by exfoliation-adsorption and in-situ intercalative polymerization. The microstructure of PAM/α-ZrP nanocomposites was confirmed by X-ray diffraction measurement, transmission electron microscopy (TEM), high resolution electron microscopy (HRTEM). The results suggested that the α-ZrP lamellae were dispersed well in PAM matrix, which indicated the formation of the exfoliated nanocomposites in the low inorganic loading of α-ZrP (≤5 wt%). With the increase of the inorganic loadings, the intercalated structure of PAM/α-ZrP nanocomposites was dominant with the d-spacings of about 1.50–1.58 nm corresponding to the inorganic loadings in the range of 10–20 wt%. Moreover, besides the electrostatic adsorption, it was also found that there may be some weak effect such as hydrogen bonding or protonation between the host and guest investigated using fourier transform infrared spectroscopy (FT-IR) and thermogravimetric (TG)analysis, which resulted in the enhancement of the thermal properties on the decomposition process of PAM/α-ZrP nanocomposites by the retardant effect of the exfoliated or intercalated α-ZrP nanometer lamellae.

R. Zhang · Y. Hu (✉) · W. Fan
State Key Lab of Fire Science, University of Science and Technology of China, Hefei, Anhui 230026, P.R. China
e-mail: yuanhu@ustc.edu.cn

B. Li · Z. Chen
Department of Chemistry, University of Science and Technology of China, Hefei, Anhui 230026, P.R. China

Introduction

Polymer/layered inorganic nanocomposites have become the focus of research in recent years because of their unique structure and excellent properties including enhanced mechanical properties, increased thermal stability and conductivity, improved gas barrier properties and reduced flammability compared with their conventional counterparts [1]. Several methods have been developed to prepare polymer/layered inorganic nanocomposites, such as exfoliation–adsorption, in situ intercalative polymerization, melt intercalation and template synthesis. However, during the past few years, much attention has been paid to the polymer/layered silicate systems because of the relatively low layer charge density and the facile exfoliation of montmorillonite-type layered silicate compounds, whereas the layered metal phosphate-based polymer composite systems have rarely been studied [2–4]. In 1995, Ding reported their work on the modification of α-ZrP using amino acids to prepare nylon6/α-ZrP nanocomposite [5], and lately, Sue and his co-workers reported their study about the preparation and fracture behavior of α-zirconium phosphate-based epoxy nanocomposites by modifying α-ZrP with monoamine-terminated polyether (Jeffamine M715) [6, 7]. Up to date, no other related research papers have been found focusing on the preparation of the polymer/α-ZrP nanocomposites.

As a kind of the synthetic layered inorganic compounds, crystalline α-ZrP was first prepared in 1964 by Clearfield and Stynes [8]. This layer structure is similar to that of montmorillonite clay. What is different is that the layers are formed by zirconium atoms connected between them by the oxygen atoms of the phosphate groups. Each phosphate contributes three of its oxygen atoms to the formation of these layers, leaving one OH group pointing

into the interlayer space. Earlier studies have shown that α-ZrP is capable of incorporating 2 mol of *n*-alkylamines with the formation of a bilayer in the interlayer space [9]. This occurs through an acid–base reaction, where the proton is transferred from the –POH group to the nitrogen or by hydrogen bonding. Also, α-ZrP has a much higher ion exchange capacity of 600 mequiv/100 g than silicate, and its quite narrow particle size distribution and high aspect ratio can be controlled by varying reaction conditions. Therefore, besides small guest molecules, polymer and even some biological macromolecules such as protein can also be inserted into the galleries of α-ZrP to obtain the nanocomposites with several improved electrical, mechanical, optical and biological properties [10–14].

Polyacrylamide (PAM) is a water-soluble polymer with wide applications in many fields such as infiltrative film [15], biosensor [16], anlistatig coat [17], nonlinear optical devices [18] and the flocculation of municipal and industrial waste [19]. On the other hand, it is attractive in fundamental research such as catalysis [20], polyelectrolytes [21] and biomedical fields [22]. Hybrids of PAM and layered inorganic compounds such as clay [23] and graphite oxide [24] have been investigated. In this study, a novel polymer nanocomposite based on the layered α-ZrP with PAM was prepared by in-situ intercalative polymerization. At the same time, the microstructure of the nanocomposites and the interaction between the host and guest were also investigated.

Experimental section

Materials

All reagents were analytical pure grade. Zirconium oxychloride octahydrate ($ZrOCl_2 \cdot 8H_2O$) and phosphoric acid (85%) were purchased from Shanghai Zhenxing Chemicals No.1 Plant. Acrylamide monomer, ammonium persulfate ($(NH_4)_2S_2O_8$) and methylamine aqueous solution (25%) were obtained from China Medicine (Group) Shanghai Chemical Reagent Corporation. All these commercial reagents were used as received without further purification.

Layered α-ZrP powder was prepared by hydrothermal synthesis under the optimum condition according to our previous work [25]. The ultrasonic treatment was carried out by a KS-900 ultrasonic generator (Ningbo Kesheng) at room temperature under an air atmosphere.

Preparation

Since the layered α-ZrP crystal has a small interlayer distance (0.76 nm) and high layer charge density, unlike layered montmorillonite, it's hard to be exfoliated in water. But, the pristine α-ZrP is facile to be exfoliated with alkylamines or alcohol amines [26, 27], by which the interlayer charge density is decreased and the interlayer distance of α-ZrP is increased, resulting in forming exfoliated colloidal phase which will be beneficial to the intercalation reaction. In this study, methylamine(MA) was chosen as a colloidal reagent for the exfoliation of α-ZrP.

To prepare PAM/α-ZrP nanocomposite, a certain amount of α-ZrP powder was dispersed in distilled water in a liquid/solid ratio of 100 mL/g, followed by adding methylamine (MA) aqueous solution of 0.2 mol/L in a mole ratio of 2.0 of amine/α-ZrP. After ultrasonic treatment for several minutes to obtain α-ZrP exfoliated phase, a desired amount of acrylamide monomer was dispersed into the exfoliated α-ZrP containing 0.5 wt% ammonium persulfate as an initiator and polymerized subsequently at 75 °C for 4 h in air. Finally, the pale yellow products were cast and dried in a vacuum oven at 60 °C for 24 h to obtain PAM/α-ZrP nanocomposites. This exfoliation-adsorption and in situ intercalative polymerization process for the preparation of PAM/α-ZrP nanocomposites can be illustrated in Fig. 1.

Characterization

X-ray diffraction (XRD) measurements were performed directly on the hybrid samples using a Rigaku D/max-rA X-ray diffractometer (30 kV, 10 mA) with Cu Kα (λ = 0.154178 nm) irradiation at a scanning rate of 0.02°/s. The transmission electron microscopy (TEM) images were obtained by H-800 microscope with an acceleration voltage of 100 kV. The high resolution transmission electronic microscopy (HRTEM) images were obtained by JEOL-2010 microscope with an acceleration voltage of 200 kV.

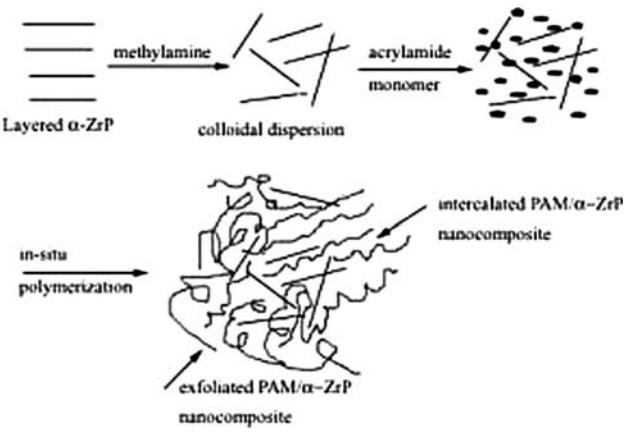

Fig. 1 Illustration of the preparation of the PAM/α-ZrP nanocomposites by exfoliation-adsorption and in situ intercalative polymerization method

The specimen for TEM and HRTEM were cut on an ultramicrotome (Ultracut UCT, Leica) equipped with a diamond knife at lower temperature to give about 70 nm thick slices. The thermal properties of the as-prepared nanocomposites were investigated by thermogravimetric(TG) analysis using a Netzsch STA-409C thermal analyzer at a heating rate of 10 °C/min under a nitrogen atmosphere.

Results and discussion

Microstructure of PAM/ α-ZrP nanocomposites

The XRD patterns of a series of PAM/α-ZrP nanocomposites with different inorganic loadings in the range of 2θ = 3–31° were shown in Fig. 2. These diffraction patterns revealed that the structure of the nanocomposites changed with the increase of the α-ZrP loadings. The common characteristic in Fig. 2 was that all patterns corresponding to the different α-ZrP loadings had a large broad hump at about 2θ = 22°, which could be assigned to the PAM matrix deriving from the intercalation and in situ polymerization of the acrylamide monomer. It is worth noticing that only one characteristic diffraction peak of PAM at 2θ = 22° could be seen in Fig. 2a corresponding to 5 wt% α-ZrP loading while the diffraction peak of the α-ZrP crystal at 2θ = 11.3° (d_{002} = 0.76 nm) disappeared because of the formation of the PAM/α-ZrP exfoliated nanocomposite. Figure 2b showed a diffraction peak at 2θ = 6.9°(d_{002} = 1.50 nm) as the α-ZrP loading increased to 10 wt%, which indicated the existence of the partially intercalated structure of the PAM/α-ZrP nanocomposite. Although the intensity of the diffraction peaks at a lower range of 2θ angle corresponding to the (002) plane of the α-ZrP intercalated by PAM molecule was enhanced gradually with the increase of the α-ZrP loading, no unambiguous change in the basal space could be seen. As for the change of the interlayer distance from 1.50 nm to 1.58 nm when the α-ZrP loading increased to 20 wt% (Fig. 2d), it was still within the error scope of XRD measure result, which did not means the difference in the structure. According to the fact that the thickness of the acrylamide molecule is 0.37 nm [5], the intercalated PAM molecule chains in the gallery of the α-ZrP may be predominantly parallel to the surface of the α-ZrP in a bilayer as schemed in Fig. 3.

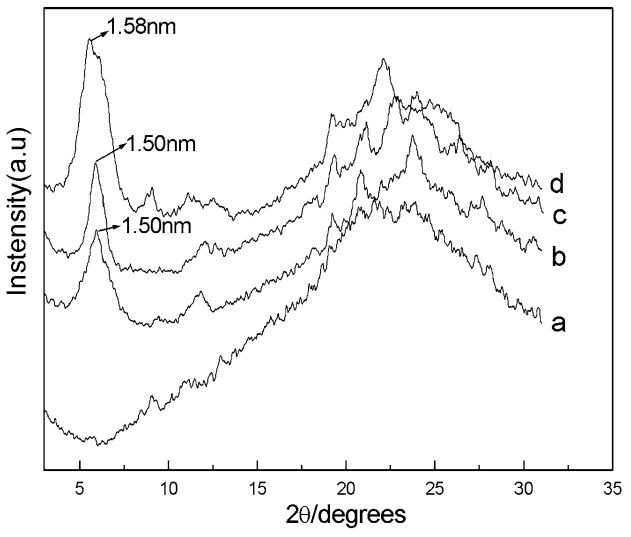

Fig. 2 XRD patterns of PAM/α-ZrP nanocomposites in different loading of α-ZrP (**a**) 5 wt%α-ZrP; (**b**) 10 wt%α-ZrP; (**c**) 15 wt%α-ZrP; (**d**) 20 wt%α-ZrP

The microstructure of PAM/α-ZrP nanocomposite was further confirmed by TEM and HRTEM observation. As shown in Fig. 4(a) and (b), the TEM images of PAM/5 wt%α-ZrP nanocomposite showed that the α-ZrP exfoliated flakes in the nanometer scale were well dispersed in the PAM matrix. At the same time, the HRTEM images of the sample shown in Fig. 5 demonstrated more clearly the state of the good dispersion and exfoliation of the α-ZrP particles in the PAM matrix. This is consistent with that of the XRD results shown in Fig. 2(a).

FT-IR spectra analysis of PAM/ α-ZrP nanocomposites

The FT-IR spectra (shown in Fig. 6) provided the changes of the characteristic absorption bands, which revealed the interaction between the polymer molecule chains and the layered α-ZrP surface in the nanocomposite. Comparing line(b) with (c), it could be seen that the C=O (carbonyl) stretching vibration at 1652 cm^{-1}shifted to 1669 cm^{-1} because of the formation of the nanocomposite while the C–C stretching vibration at 1616 cm^{-1} unchanged. The reason was that there may be some interaction between the host (α-ZrP) and the guest (PAM) through P–O–H·····O=C type hydrogen bonding [12], which strengthened the C=O stretching vibration. Also, the disappearance of the C=C stretching vibration at 1708 cm^{-1} indicated no remained

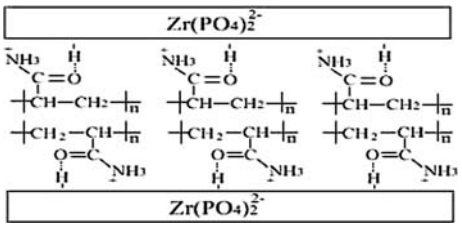

Fig. 3 Scheme of the arrangement of PAM chains between the interlayer of α-ZrP

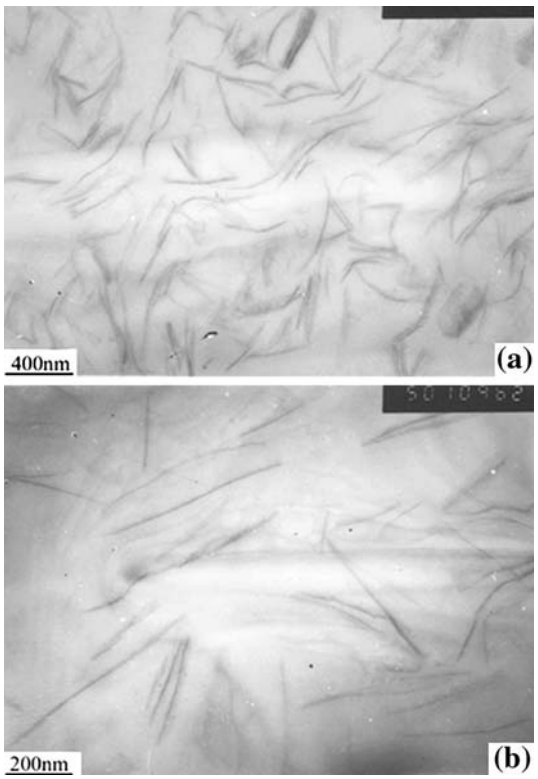

Fig. 4 TEM images of PAM/5 wt%α-ZrP nanocomposite

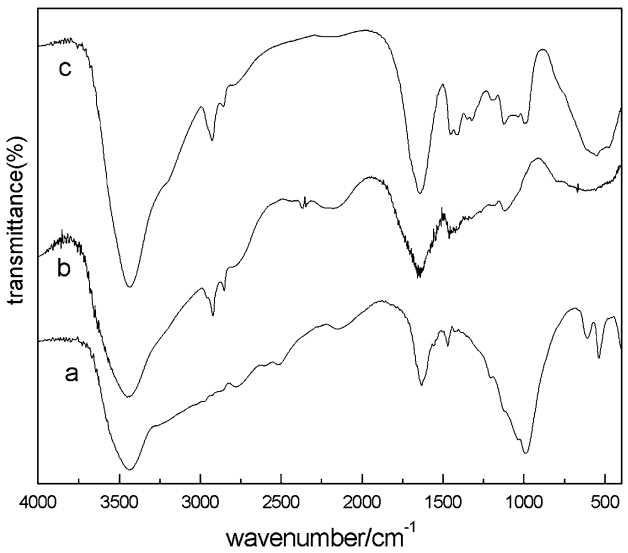

Fig. 6 FTIR spectra of the samples for (**a**) α-ZrP; (**b**) PAM and (**c**) PAM/α-ZrP nanocomposite

acrylamide monomer after polymerizing. At the same time, due to the protonation or formation of the hydrogen bonding between the $–NH_2$ in PAM and the P–OH in α-ZrP, the N–H stretching vibration may be weakened which resulted in the shifts of the absorption bands from 3419 to 3385 cm^{-1} and 3205 to 3194 cm^{-1}, respectively [9]. The changes of the absorption bands from 1112 cm^{-1} to 1122 cm^{-1} and from 1180 to 1194 cm^{-1} may be due to the reinforcement of the C–N stretching vibration. In addition, comparing line (a) with (c), it could be found that the absorption bands at 1048 and 1121 cm^{-1} attributing to the characteristic absorption of PO_4 in α-ZrP shifted to 984 and 1033 cm^{-1}, respectively, which indicated a certain interaction between the $CONH_2$ and the P–OH. Therefore, as provided by FT-IR spectra, it could be suggested that there is not only an electrostatic adsorption effect between the PAM and α-ZrP, but also some weak interaction such as hydrogen bonding or protonation as schemed in Fig. 3.

Fig. 5 HREM images of PAM/5 wt%α-ZrP nanocomposite

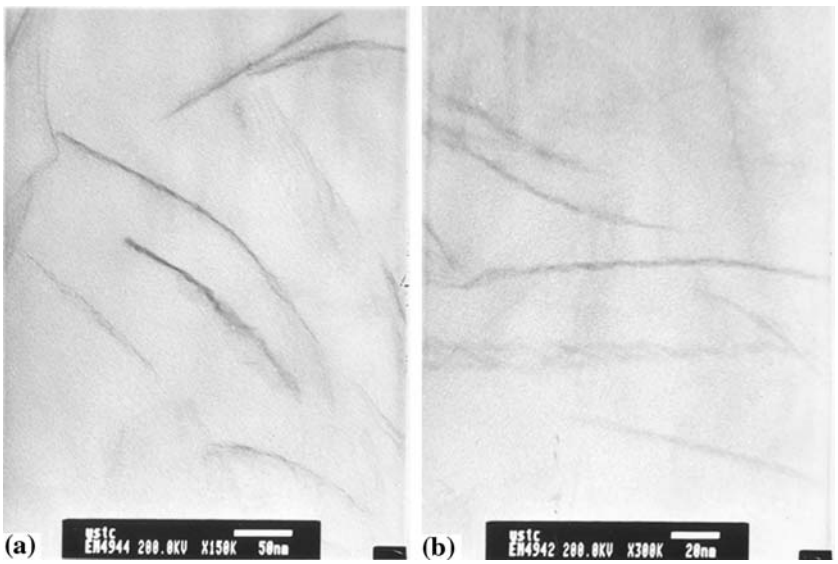

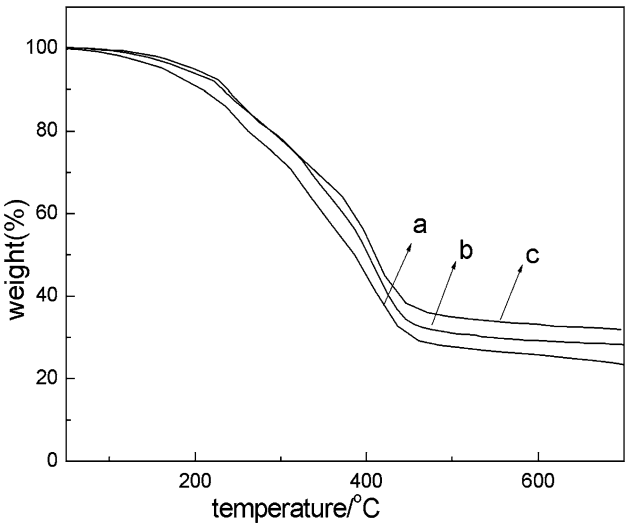

Fig. 7 TG curves of (**a**) pure PAM; (**b**) PAM/5 wt%α-ZrP and (**c**) PAM/15 wt%α-ZrP nanocomposites

Thermal stability of PAM/ α-ZrP nanocomposites

The thermogravimetric (TG) curves and analysis results of the PAM and its nanocomposites with different α-ZrP loadings were shown in Fig. 7 and listed in Table 1, respectively. When the 5% weight loss is selected as a comparison point, the start decomposition temperatures ($T_{d\text{-}5\%}$) of PAM/α-ZrP nanocomposites were higher than those of pure PAM. When the 50% weight loss was selected as a comparison point, there was a similar trend on the changes of the decomposition temperatures ($T_{d\text{-}50\%}$) compared with $T_{d\text{-}5\%}$. Meanwhile, the charred residues at 600 °C increased with the increase of the inorganic loadings in the nanocomposites as shown in Table 1. These results suggested that the thermal decomposition process and the thermal properties of the nanocomposites were improved because of the effect of the layered α-ZrP lamellae in the matrices. The elucidation for this effect in the enhancement of the thermal stability included the following two aspects. First, during the process of the thermal decomposition, a desired energy was needed to overcome the protonation or the hydrogen bonding effect between the $–CONH_2$ in PAM and the P–OH in α-ZrP. Second, the evaporation and escape of the thermal decomposed product molecules and the heat transfer from the thermal degradation of the PAM molecule in the confined gallery were retarded due to the dispersion of α-ZrP exfoliated or intercalated nanometer sheets. These two effects simultaneously resulted in the enhancement of the thermal properties of PAM/α-ZrP nanocomposites.

Table 1 TGA results of pure PAM and PAM/α-ZrP nanocomposites

Samples	Td (–5%)/°C	Td (–50%)/°C	Char/% (at 600 °C)
(a) pure PAM	182	398	23.32
(b) PAM/5 wt%α-ZrP	183	405	27.3
(c) PAM/15 wt%α-ZrP	198	411	34.1

Conclusions

PAM/α-ZrP nanocomposites were successfully synthesized by exfoliation-adsorption and in-situ intercalative polymerization. TEM and HRTEM images showed that the α-ZrP lamellae were dispersed well in PAM matrix and the exfoliated nanocomposite was formed corresponding to the 5 wt% α-ZrP, which is consistent with the result of XRD measurement. Although the intensity of the diffraction peaks at a lower range of 2θ angle corresponding to the (002) plane of the α-ZrP intercalated by PAM molecule was enhanced gradually with the increase of the loading of α-ZrP from 10 to 20 wt%, no unambiguous change in the interlayer distances of the nanocomposites could be seen. Moreover, besides the electrostatic adsorption, there may be some weak interaction such as hydrogen bonding or protonation between the host and guest investigated using FT-IR and TG analysis. As a result, the thermal stability of the nanocomposites was improved by the retardant effect of the exfoliated or intercalated α-ZrP nanometer lamellae.

Acknowledgement The work was financially supported by the China NKBRSF project (No.2001CB409600), the National Natural Science Foundation of China (No.50323005) and (No.50476026).

References

1. Alexandre M, Dubois P (2000) Mater Sci and Eng 28:1
2. Lebaron PC, Wang Z, Pinnavaia TJ (1999) Appl clay sci 15:11
3. Albrecht M, Ehrles S, Muhlebach A (2003) Macromol Rapid Commun 24:382
4. Kong QH, Hu Y, Lu HD, Chen ZY, Fan WC (2005) J Mater Sci 40:4505
5. Ding Y, Jones DJ, Maireles-Torres P, Roziere J (1995) Chem Mater 7:562
6. Sue HJ, Gam KT (2004) Chem Mater 16:242
7. Sue HJ, Gam KT, Bestaoui N, Clearfield A, Mioyamoto M, Miyatake N (2004) Acta Materialia 52:2239
8. Clearfield A, Stynas JA (1964) J Inorg Nucl Chem 26:117
9. Maclachian DJ, Morgan RK (1992) J Phys Chem 96:3458
10. Nunes LM, Airldi C (1999) Chem Mater 11:2069
11. Kumar CV, Chaudhari A (2000) J Am Chem Soc 122:830
12. Chao KJ, Chang TC, Ho SY (1993) J Mater Chem. 3:427
13. Kumar CV, Chaudhari A (2001) Chem Mater 13:238
14. Jin W, Brennan JD (2002) Analytica Chimica Acta 461:1
15. Okamoto M, Morita S, Kim YH, Kotaka T, Tateyama H (2001) Polymer 42:1201
16. Decher G, Lehr B, Lowach K, Lvov Y, Schmitt J (1994) Biosensors Bioelectronics 9:677

17. Cheung JH, Fou AF, Rubner MF (1994) Thin Solid Films 244:985
18. Laschewsky A, Mayer B, Wischerhoff E, Arys X, Bertrand P, Jonas A, Delcorte A, (1996) Thin Solid Film 284–285:334
19. Hao JC, Zheng LQ, Li GZ, Wang HQ, Du ZW (1996) Polymer 37:3117
20. Jose L, Pillai VNR (1996) Eur Polym J 32:1431
21. Churchman GJ (2002) Appl Clay Sci 21:177
22. Kim SR, Yuk SH, Jhon M (1997) Eur Polym J 33:1009
23. Yeh JM, Liou SJ, Y.W.Chang (2004) J App Polym Sci 91:3489
24. Xu JY,Hu Y, Song L, Wang QA, Fan WC (2001) Res Bull 36:1833
25. Zhang R, Hu Y, Song L, Zhu YR, Fan WC, Chen ZY (2001) Chinese J Nonferr Metals 11:895
26. Xu JS, Tong Y, Zhang H, Z Gao (1997) Chem J Chinese Universities 18:88
27. Espina A, Menéndez F, Jaimez E, Khainakov SA, Trobajo C, García JR (1998) Mater Res Bull 33:763